Jahresbericht 2003, 10. Dezember 2003

Projekt Nr. 43099

Large Eddy Simulation für die turbulente, nicht vorgemischte Verbrennung

Autor und Koautoren	Marco Küng[1)], Steffen Stolz[2)], Christos Frouzakis[1)], Ananias Tomboulides[1)] Sevket Baykal[3)], Jürg Gass[3)] Julian T. Becerra Sagredo[4)], Rolf Jeltsch[4)]
beauftragte Institution	1) Labor für Aerothermochemie und Verbrennungssysteme (LAV) 2) Institut für Fluiddynamik (IFD) 3) Labor für Thermodynamik in neuen Technologien (LTNT) 4) Seminar für angewandte Mathematik (SAM)
Adresse	ETH Zürich ETH Zentrum CH-8092 Zürich
Telefon, E-mail, Internetadresse	vgl. die folgenden Berichte!
BFE Projekt-/Vertrag-Nummer	43099 / 83050
Dauer des Projekts (von – bis)	November 2001 bis November 2004

ZUSAMMENFASSUNG

Am Projekt sind 4 Gruppen beteiligt, welche die Thematik in zwei parallelen Teilvorhaben angehen: i) LAV und IFD sowie ii) LTNT und SAM. Etwa zwei Drittel der Projektdauer sind verstrichen und der Projektstand der beiden Teile i) und ii) ist im folgenden beschrieben:

i) LAV und IFD: Das Projekt, in dem eine turbulente Diffusionsflamme mittels Grobstruktur-Simulation (LES) berechnet werden soll, wurde zu Beginn in 3 Teilprojekte aufgeteilt: 1.) Inkompressible LES einer Kanalströmung; 2.) Kompressible (für kleine Mach-Zahlen) LES eines runden Jets mit Mischung und veränderlicher Dichte, aber ohne chemische Reaktionen; 3.) LES einer kompressiblen (für kleine Mach-Zahlen) und turbulenten Diffusionsflamme.In den vergangenen 12 Monaten konnte, nach anfänglichen Problemen des LES-Programmteils, Teilprojekt 1 beendet werden, in welchem die inkompessible Kanalströmungen für eine Reynolds-Zahl von 2800 simuliert wurde. Die Resultate (Wand-Reynoldszahl, gemitteltes Geschwindigkeitsprofil in Strömungsrichtung und die Reynolds-Spannungen) zeigen eine gute Übereinstimmung mit exakten Ergebnissen der Direkten Numerischen Simulation. Mit dem Abschluss des Teilprojektes 1 ist auch die Implementierung des LES-Modells für die Strömung abgeschlossen. Zur Zeit resultiert daraus ein Verzug von ca. 6 Monaten zum Projektplan. Wir sind aber optimistisch, dass in den nächsten 6 Monaten (Monate 25 – 30 des Projektes) das Teilprojekt 2 und in den Monaten 31-36 des Projektes das Teilprojekt 3 abgeschlossen werden können. Als Vorarbeit zum Teilprojekt 2 wurde einerseits eine Literaturstudie und andererseits erste Tests mit vermischenden Strahlen durchgeführt.

ii) LTNT und SAM: Einerseits wurde am SAM eine neue, mehrdimensionale Lagrange-Transport-Methode (LTM) hoher Ordnung entwickelt. Die neue Methode basiert auf Darstellungen von Strömungselementen als Langrange'sche Finite Volumina, die bewegt und deformiert werden. Explizite kardinale Z-Spline-Interpolation wurde für die Darstellung der Strömungselemente und für die Interpolation auf ein festes numerisches Gitter benutzt. Die LTM wurde zur Integration der Kompressiblen Strömungsgleichungen benutzt. Mit der Technik der Grobstruktursimulation (LES) wurde ein dynamisches Subgitter-Modell der kinetischen Energie von Turbulenzen einbezogen. Die Verbrennung wurde mit Lagrange'schen Wahrscheinlichkeitsdichtefunktionen simuliert. Diese reduzieren erheblich die zur Beschreibung der wichtigen, chemischen Reaktionen nötigen Grössen.

Andererseits wurde vom LTNT ein transienter Flamelet-Code in die komerzielle Software CFX5.6 implementiert und getestet, welcher in einer nächsten Phase in den Code vom SAM implementiert werden soll.

Somit ist einerseits der kompressible Code für die Fluiddynamik (vom SAM) sowie ein Flamelet-Model (vom LTNT) fertiggestellt und die beiden Programme können im nächsten Schritt zu einem gemeinsamen Programm zur Grobstruktusimulation von Diffusionsflammen vereint werden.

BFE OFEN UFE SFOE

3. Diffusion Jet Flame Large Eddy Simulation with an Approximate Deconvolution Model (ADM)

Marco Küng [1)], Steffen Stolz[2)], Christos Frouzakis[1)], Ananias Tomboulides[3)]

1) Laboratory of Aerochemistry and Combustion Systems LAV
2) Institute of Fluid Dynamic IFD
3) University of Thessaloniki (Greece)

LAV
8092 Zürich, Switzerland
http://www.lav.ethz.ch
kueng@lav.mavt.ethz.ch

8th December 2003

1 Summary and Outlook

The Large Eddy Simulation (LES) project for diffusion flame calculation is splitted in 3 parts:

1. LES of incompressible channel flow
2. LES of compressible (for low Mach numbers) and turbulent axisymmetric jet with mixing, variable density and the absence of chemical reactions
3. LES of compressible (for low Mach numbers) and turbulent jet diffusion flame

The motivation behind this splitting is that the validation of different processes can be done separatly: i) turbulent momentum diffusion (part 1), ii) turbulent diffusion of passive scalars and the influence of the variable density on the momentum of the jet (part 2) and iii) the chemical source term modelling (part 3).
During the past 12 months, part 1 could be completed, however, problems with the LES-model implementation in the code have been occurrenced. Incompressible channel flow simulations are performed for a Reynolds number of $Re = 2800$. The results e.g. friction Reynolds number, mean velocity profile in streamwise direction and the Reynold stresses are in good agreement with accurate data from direct numerical simulation. Therefore the implementation of the LES model for the fluid dynamics part can be condluded.
At the moment there is a delay of arround 6 month in comparison with the original timeplan, however, we are optimistic to finish part 2 and therefore compensate the delay during the next 6 months. A literature study about mixing jets, first tests with the setup and the forcing of the jet are done as a preliminary work for part 2.

2 Governing Equations

The set of Favre-averaged LES equations with the approximate deconvolution model (ADM) [20] are derived by Küng [12] for low Mach number flows including chemical reactions. All quantities are normalized and $\underline{u}$ is the velocity vector, T the temperature, Y_i the mass fraction of species i, p_2 the hydrodynamic pressure, ρ the density, μ the dynamic viscosity, c_p the specific heat, λ the heat conductivity, $\dot{\omega}$ the chemical source term, D the species diffusion coefficient, $\underline{\underline{S}}$ the strain rate tensor, Re the Reynolds number, Sc the Schmidt number, Pr the Prandtl number, Da the Damkoehler number, i denotes the species, I is a unity matrix, G the LES filter-operator, Q_n the approximate inverse of G, χ the relaxation factor,and overbar "$\bar{.}$" denotes LES filtering, "$\tilde{.}$" means favre averaging and * denotes a deconvoluted quantity.

Temperatur equation with ADM

$$\overline{c}_p\overline{\rho}\left[\frac{\partial\widetilde{T}}{\partial t}+\underline{u}^\star\cdot\widetilde{(\nabla T^\star)}\right]=\frac{1}{RePr}\nabla\cdot\left[\widetilde{\lambda}(\nabla\widetilde{T})\right]-Da\sum_i\overline{h_i^0\dot{\omega}_i}-\overline{c}_p\overline{\rho}\chi_T(I-Q_N*G)*\widetilde{T} \tag{1}$$

Species equation with ADM

$$\overline{\rho}\Big[\frac{\partial\widetilde{Y}_i}{\partial t}+\underline{u}^\star\cdot\widetilde{(\nabla Y_i^\star)}\Big]=\frac{1}{ReSc_i}\Big[\Delta(\overline{\rho}\widetilde{D_{i,ref}}\widetilde{Y}_i)-\overline{\rho}\widetilde{Y}_i\underline{\widetilde{u}}_c\Big]+Da\overline{\dot{\omega}}_i-\overline{\rho}\chi_{Y_i}(I-Q_N*G)*\widetilde{Y}_i \tag{2}$$

Momentum equation with ADM

$$\overline{\rho}\Big[\frac{\partial\underline{\widetilde{u}}}{\partial t}+\underline{u}^\star\widetilde{(\nabla\cdot\underline{u}^\star)}\Big]+\nabla\overline{p}_2=\frac{1}{Re}\nabla\cdot(\tilde{\mu}\underline{\underline{\tilde{S}}})+\frac{1}{Fr^2}\overline{\rho}\underline{e}_g-\overline{\rho}\chi_u(I-Q_N*G)*\underline{\widetilde{u}} \tag{3}$$

with

$$\underline{\underline{\widetilde{S}}}=\nabla\underline{\widetilde{u}}+(\nabla\underline{\widetilde{u}})^T-\frac{2}{3}(\nabla\cdot\underline{\widetilde{u}})\underline{\underline{I}} \tag{4}$$

Continuity equation with ADM

$$\nabla\cdot\underline{\widetilde{u}}=\frac{1}{\overline{c}_p}\left\{\frac{1}{RePr}\nabla\cdot[\widetilde{\lambda}(\nabla\widetilde{T})]-Da\sum_i\overline{h_i^0\dot{\omega}_i}-\overline{c}_p\overline{\rho}\chi_T(I-Q_N*G)*\widetilde{T}\right\}-\overline{\rho}\Big[\underline{u}^\star\cdot\widetilde{(\nabla T^\star)}-\underline{\widetilde{u}}\cdot(\nabla\widetilde{T})\Big] \tag{5}$$

Equation of state

$$1=\overline{\rho}\widetilde{T} \tag{6}$$

3 LES of turbulent channel flow

In this chapter we consider LES of a turbulent channel flow with the assumption of an incompressible fluid consisting of one species with constant properties and the absence of bouyancy and chemical reactions. For an introduction and some reviews of turbulent channel flows we may refer to Pope [16]. For this case, the set of equations (1) to (6) reduces then only to the continuity- and the momentum equations

$$\nabla \cdot \underline{\overline{u}} = 0 \tag{7}$$

$$\frac{\partial \underline{\overline{u}}}{\partial t} + \overline{(\underline{u}^\star \cdot \nabla)\underline{u}^\star} - \nabla \overline{P} = \frac{1}{Re}\nabla^2 \underline{\overline{u}} - \chi_u (I - Q_N * G) * \underline{\overline{u}} \tag{8}$$

where $P = p_2/\rho$. We consider fully developed channel flow simulations with periodic boundary conditions in streamwise- and spanwise- direction (figure 1). At the walls no slip conditions are imposed for the velocity. Simulations are performed for $Re_\tau = \frac{u_\tau \delta}{\nu} \approx 180$, where δ is the channel half width and

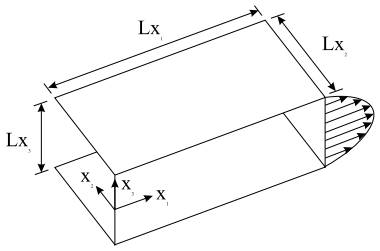

Figure 1: Sketch of channel flow with the Cartesian coordinate system: x_1 (streamwise), x_2 (spanwise) and x_3 (wall-normal)

$$u_\tau = \sqrt{\frac{\tau_w}{\rho}} \tag{9}$$

$$\tau_w = \rho\nu\Big(\frac{\partial \overline{u}_1}{\partial x_3}\Big)_{wall} \tag{10}$$

where Re_τ is called friction Reynolds number, u_τ friction velocity and τ_w wall shear stress. Note, that $Re = \frac{u_\infty \delta}{\nu} = 2800$, where u_∞ is the bulk velocity is fixed and Re_τ is the result of the simulations. The ratio δ/u_∞ yields the used timescale (or time unit). The simulations are forced in x_1-direction for a constant x_1-mass flux. The computational domain with the size of $Lx_1 \times Lx_2 \times Lx_3 = 4\pi \times 4\pi/3 \times 2$ is discretized with a grid of 6 spectral elements in each of the directions. The spectral elements are distributed uniform in streamwise- and spanwise-direction and are distributed nonuniform in wall normal direction, where the spectral element distribution in is transformed with $sin(2x_3\pi)$. The number of collocation points per spatial direction inside an element was set equal 9. For all calculations the timestep is set equal 1/100 of the timescale. The statistically stationary LES-results are averaged in x_1 x_2 planes and time. Results for both channel halfes are plotted. The LES results of the mean velocity and the Reynolds stresses are compared with unfiltered DNS-data from Moser et al. [14]. The goals of this chapter are i) an investigation of the sensitivity on the relaxation parameter χ_u and ii) validation of the ADM-formulation in a spectral element code with respect to Re_τ, mean velocity and Reynold stresses.

3.1 Investigation of the relaxation parameter χ_u

The relaxation term $\chi_u(I - Q_N * G) * \underline{\overline{u}}$ on the right hand side of (8) can be interpreted as a term, which extracts energy from the large scales (for $\chi_u > 0$) and transfer it to small non-resolved scales. The determination of χ_u includes the whole challange of turbulence modelling. To stabilize turbulent flow calculations in spectral element codes, Fischer et al. [8] proposed a low pass-filter. In the following this filter is called "spectral element-filter" (SE-filter). The SE-filter touches only the Lagrange polynomial coefficient of the highest order.
In this chapter the relaxation parameter χ_u is investigated in combination with and without the SE-filter. The parameters are varied, according to table 3.1 and the simulation results of Re_τ are plotted in figure 2. It is obvious from figure 2 it is obvious, that Re_τ is not sensitiv in the range of $8 \leq \chi_u \leq 60$ and the simulations with and without SE-filter gives the same Re_τ. If χ_u is more decreased, less energy is extracted from system and the simulations become unstable (for the case without the SE-filter) or the steepness of the streamwise-velocity at the wall will be increased with the consequence of a higher Re_τ (for the case with the SE-filter). A large value of χ_u causes to a laminarisation of the channel flow.

χ_u	Re_τ(without SE-filter)	Re_τ (with SE-filter)
4	-	182
6	-	175
8	175	177
9	175	176
10	174	175
18	173	172
22	173	174
40	173	173
50	173	172
60	173	173
90	170	170
no SGS-LES	-	183

Table 1: Parameters and results of the χ_u investigation.

In addition the mean streamwise velocity profile, the velocity fluctuations and the Reynolds stresses are shown for $\chi_u = 8$ and $\chi_u = 40$ with and without filter and for an LES without a subgrid scale model (SGS model). This results are not yet absolutely stastic stationary and the simulations has to be continueed.
The mean velocity profiles, with x_3 scaled in outer units and in wall units, obtained with LES and χ_u-values of 8 and 40 are displayed together with the unfiltered DNS data from Moser et al. [14] in the upper plots of figures 3, 4, 5 and 6. The results of the LES without SGS-model are displayed in the upper plots of figure 7. For alle LES cases a relatively good agreement between LES and unfiltered DNS is observed. The LES without SGS-model undershoots the correct wall-law due to missing SGS dissipation.
The root-mean-square of the velocity fluctuations $u_i' = u_i - < u_i >$ is shown in the lower left plots of figures 3, 4, 5 and 6. The fluctuations of the streamwise velocity component are plotted with solid lines, those of the spanwise component with dashed lines and those of the wall-normal component with dotted lines. The overall agreement between LES and unfiltered DNS is relatively good but does underpredict the DNS exept in the range of the maximum value of the streamwise component where the LES overshoots the unfiltered DNS data. Note, that the root-mean-square of the velocity fluctuations ar expected to be smaller for the LES due to the spatial filtering. In contrast to the LES results, the no-SGS LES overpredicts the fluctuations. The Reynolds stresses $< u_1' u_3' >$, presented in the lower right plots of figures 3, 4, 5 and 6 shows the same trends as the normal Reynolds stresses. According to figure 2 the simulations with SE-filter allows lower values of χ_u but the influence on the mean velocity and the Reynolds stresses are negligible in comparison with the results without SE-filter.

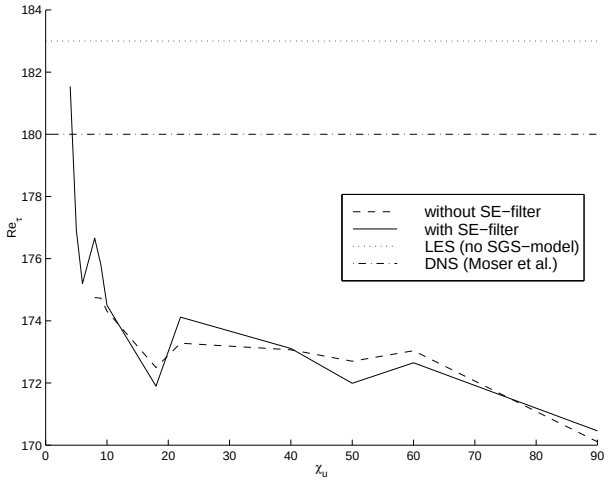

Figure 2: Averaged Re_τ as a function of a constant relaxation parameter χ_u

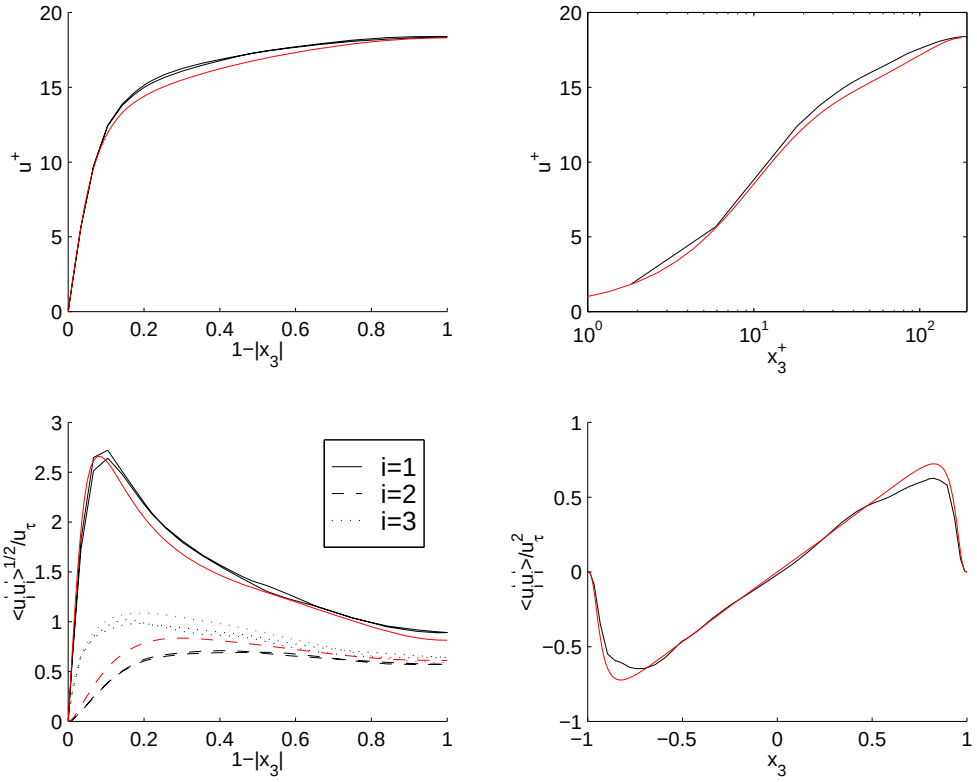

Figure 3: Velocity profile scales with u_τ, upper left: linear plot, upper right: logarithmic plot, lower left: velocity fluctuations and lower right: Reynolds stresses for $Re_\tau \approx 180$, black lines: LES with $\chi_u = 8$ and without SE-filter, red (grey) lines: DNS from Moser et al. [14]

3.2 Conclusions

Incompressible channel flow simulations are performed for a Reynolds number of $Re = 2800$. The results, e.g. friction Reynolds number, mean velocity profile and the Reynolds stresses are in good agreement with accurate DNS-data. The results are not yet absolutly statistic stationary and the simulations has to be continued. However, the implementation of the LES-model for the fluid dynamics part can bi concluded.

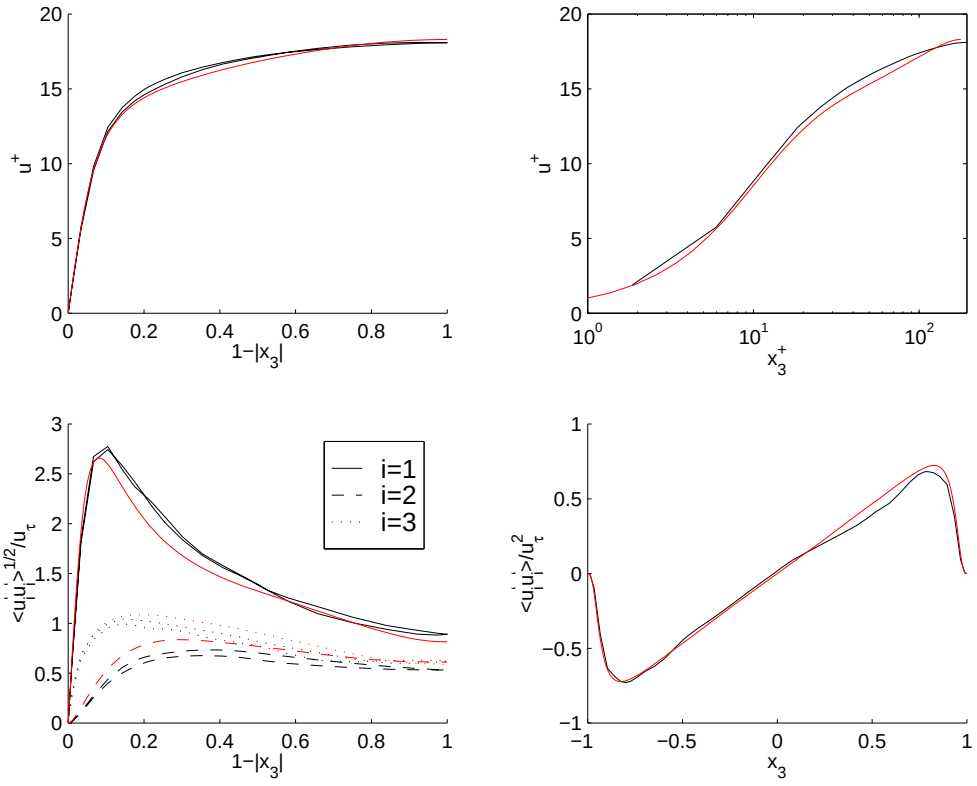

Figure 4: Velocity profile scales with u_τ, upper left: linear plot, upper right: logarithmic plot, lower left: velocity fluctuations and lower right: Reynolds stresses for $Re_\tau \approx 180$, black lines: LES with $\chi_u = 8$ and with SE-filter, red (grey) lines: DNS from Moser et al. [14]

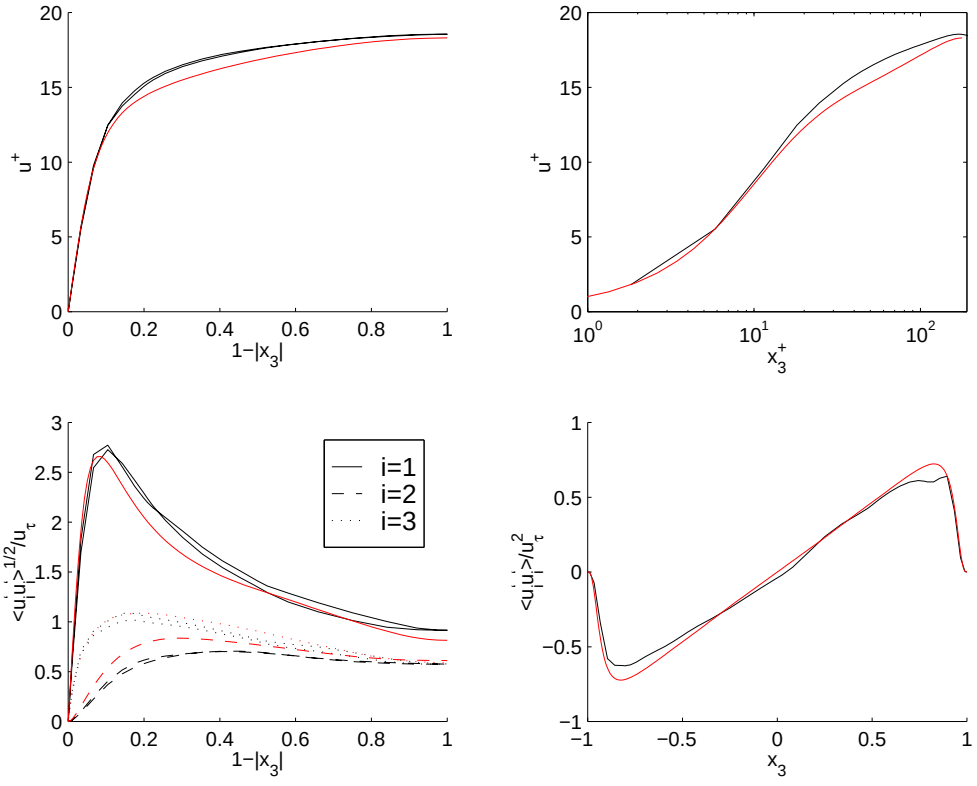

Figure 5: Velocity profile scales with u_τ, upper left: linear plot, upper right: logarithmic plot, lower left: velocity fluctuations and lower right: Reynolds stresses for $Re_\tau \approx 180$, black lines: LES with $\chi_u = 40$ and without SE-filter, red (grey) lines: DNS from Moser et al. [14]

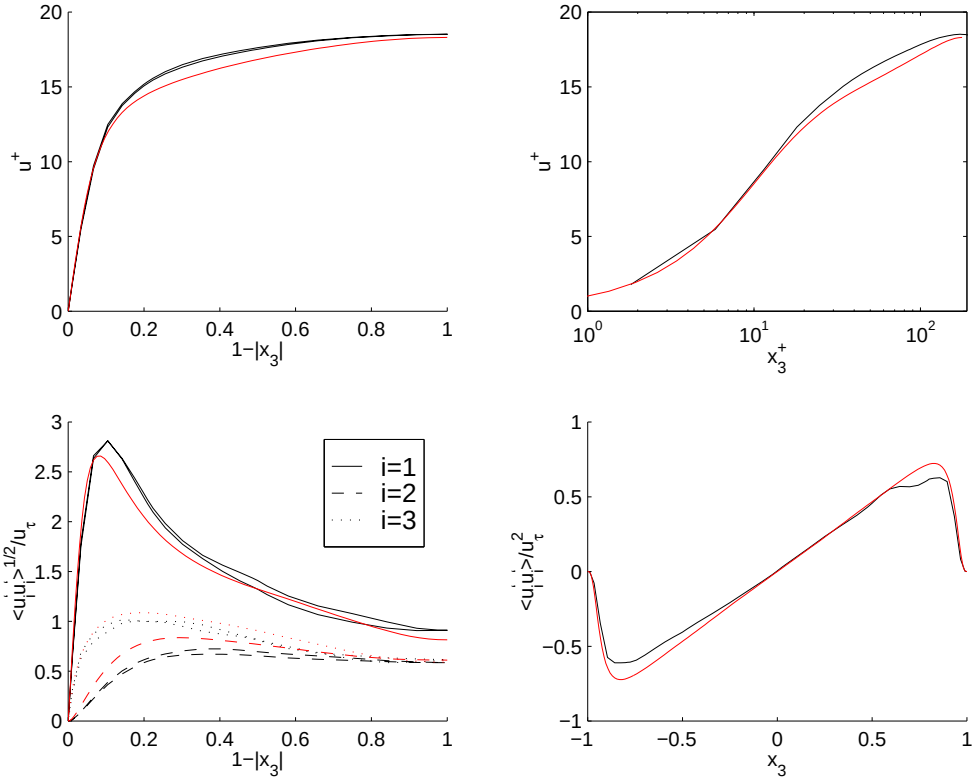

Figure 6: Velocity profile scales with u_τ, upper left: linear plot, upper right: logarithmic plot, lower left: velocity fluctuations and lower right: Reynolds stresses for $Re_\tau \approx 180$, black lines: LES with $\chi_u = 40$ and without SE-filter, red (grey) lines: DNS from Moser et al. [14]

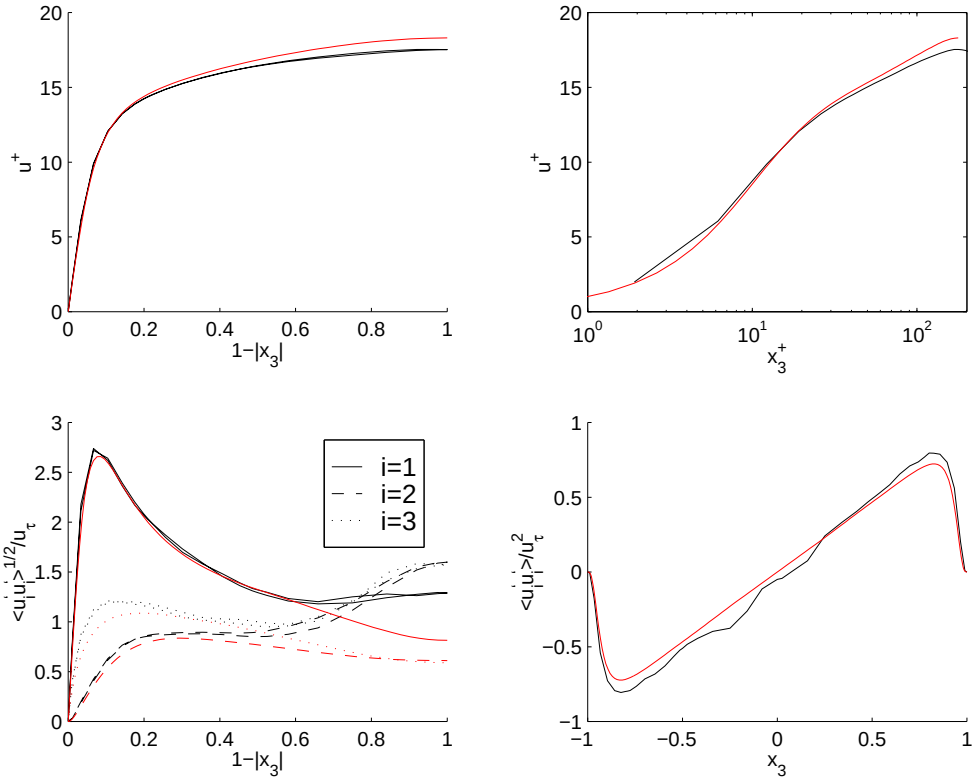

Figure 7: Velocity profile scales with u_τ, upper left: linear plot, upper right: logarithmic plot, lower left: velocity fluctuations and lower right: Reynolds stresses for $Re_\tau \approx 180$, black lines: no SGS-LES, red (grey) lines: DNS from Moser et al. [14]

4 LES of the mixing of a passive scalar in a turbulent jet

4.1 Literatur Review

The dynamic of turbulent round jets have been studied extensively in the literature. For some introduction consult Pope [16]. Wygnanski et al. [22] performed a comprehensive study of the self-similar region of the round jet and reported moments, energy balance, intermittency microscales and integral lengths. Using a new method of analysing hot-wire signals, Rodi et al. [17] made measurements of mean velocity and turbulent intensities and showed that the mean velocity decay along the axis of the jet conformed to the x^{-1} decay expected from similarity analysis, unlike the measurements of Wygnanski et al. [22]. Seif et al. [19], analysing the data of both Wygnanski et al. [22] and Rodi et al. [17], found a significant shortfall in the momentum flux across the jet. Capp et al. [4] and George et al. [9] hypothesized that a return flow that might be set up in the entrainment regions of the jet facility may explain this lack of conservation of momentum and derived a criterion relating the volume flux of the jet and the room size to the expected momentum loss with distance. Panchapakesan et al. [15] investigated with laser-Doppler (LDA) measurements the axisymmetric jet of air and helium and measured moments of velocity fluctuations up to fourth order. Hussein et al. [11] undertook laser-Doppler (LDA) measurements and stationary hot-wire (SHW) measurements in a round jet with nozzle exit conditions close to that of Wygnanski et al. [22] but in a much larger room, to emulate a jet in an infinite environment. Significant differences between the LDA and SHW measurements of Hussein et al. [11] are observed, especially in higher order moments.
Recently, it has become possible to study the dynamic of turbulent flow by means of numerical simulation. Boersma et al. [2] investigated the effect of inflow conditions of an axisymmetric jet to the similarity of the jet in a direct numerical simulation (DNS) of an axisymmetric turbulent jet and compared their results extensively with the measurements of Hussein et al. [11] and Panchapakesan et al. [15].

Apart from its dynamics, turbulent jet flow have been also studied for its mixing properties. Together with the fluid flow one may also emit a substance from the orifice which is then dispered by the turbulence. The substance is taken to be passive, which means that it does not contribute to the jet dynamics. Turbulent mixing in jet flow has been investigated by experimental methods in many studies, e. g. by Corrosin et al. [5] who used a hot-wire anemometer to detect temperatur fluctuations. Becker et al. [1] investigated the concentration field of the round turbulent jet. Dowling et al. [7] investigated the similarity of the concentration field at different Reynolds numbers. They found that the mean concentration profile is self-similar and independent of Reynolds number which they call general similarity. The root mean square of the fluctuations of the concentration and the probability density function of the concentration were found to be self-similar with a dependence of the Reynolds numbers which they call specific similarity. Scheffer et al. [18] investigated the role of large-scale structure in the mixing of a non-reacting turbulent CH_4 jet.
From a theoretical point of view mixing a turbulent jet flow has been mainly treated in terms of self-similarity theory. An overview of self-similarity of concentration profiles may be found in Hinze [10].
In addition to the experimental and theoretical studies of mixing in turbulent jet flow quoted above numerical simulations of such flows have been performed. Most of these numerical studies have concentrated on the transition process from laminar to turbulent region close to the jet orifice. An example of such a study is from Danaila et al. [6]. Boersma et al. [2] considered the fully developed jet and investigated the scale similarity range. Lubbers et al. [13] were the first, which performed a DNS of a turbulent jet in combination with the mixing of a passive scalar and did concentrate on the self-similarity of passive scalar concentrations and compared it extensively with experimental data.

4.2 Numerical Implementation

In Fig. 8 a sketch of the axisymmetric round jet geometry and the Cartesian coordinate system is showed. The geometrical configuration simulates a round jet issuing from a circular orifice of diameter $d = 2r_0$ with species $i = 1$ in free space, i.e. without confining walls. The orifice is surrounded by a coflow with a coflow velocity u_{co} and species $i = 2$. The velocity scale is given by the difference of the (approximately) flat-topped velocity in stream wise direction u_j and the coflow velocity u_{co}. The ratio $d/(u_j - u_{co})$ yields the used time scale.
The three-dimensional calculations are performed in Cartesian coordinates in a cylindrical computational domain. The flow is assumed to be an isothermal 2-species flow with the absence of bouyancy and chemical reactions. Further it is assumed, that both species have identical properties which are fixed to be constant. According to the equations (1) to (6) this case is governed by the following equations for the conservation of mass, momentum and species

$$\nabla \cdot \underline{\overline{u}} = 0 \tag{11}$$

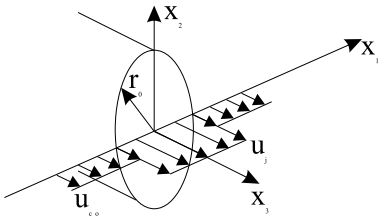

Figure 8: Sketch of the axisymmetric jet flow

$$\frac{\partial \overline{\underline{u}}}{\partial t} + \overline{\underline{u}^{\star}(\nabla \cdot \underline{u}^{\star})} + \nabla \overline{p}_2 = \frac{1}{Re}\nabla \cdot \underline{\underline{\tilde{S}}} - \chi_u (I - Q_N * G) * \overline{\underline{u}} \tag{12}$$

$$\left[\frac{\partial \overline{Y}_i}{\partial t} + \overline{\underline{u}^{\star} \cdot (\nabla Y_i^{\star})}\right] = \frac{1}{ReSc_i}\left[\Delta(\overline{D_{i,ref}}\ \overline{Y}_i) - \overline{Y}_i \overline{\underline{u}}_c\right] - \chi_{Y_i}(I - Q_N * G) * \overline{Y}_i \tag{13}$$

For the initial velocity profile of the orifice an artificial profile in streamwise direction is used

$$u(x) = \frac{u_j - u_{co}}{2} + \frac{u_j - u_{co}}{2} tanh\left[\alpha\left(\frac{1}{r} - r\right)\right] \tag{14}$$

with radius $r = \sqrt{x_1^2 + x_2^2}$ and the steepness parameter α respectively. The Schmidt numbers Sc_i used in the simulations are according to Lubbers et al. [13] set equal 1.0, the Reynolds number, based on the orifice diameter d and the velocity difference $u_j - u_{co}$ is $Re = 2.0 \times 10^3$ and the velocity ratio u_j/u_{co} is equal 2.0. LES of axisymmetric mixing jets will be performed in the next 6 month of the project. The scale similarity LES results of the mean profiles and the the Reynolds stresses of the streamwise velocity and the Y_1-concentration will be compared with unfiltered DNS-data from Lubbers et al. [13].
In the next chapter and as a preliminary first step turbulent round jets are investigated by means of Direct Numerical Simulations (DNS). The advantage to do this over LES is that the DNS-code is well established (stable, ...).

4.3 Preliminary DNS-tests

In turbulent jet simulations, the flow has to be perturbed in order to become turbulent. In experimental studies this is not necessary, as different small distubances are allways present. However, in well resolved simulations no disturbances (exept for the roundoff error) trigger the transition of the jet.
Here, the perturbation of the jet is done by a three dimensional random force, which is applied in a small region in the shear layer of the jet close to the orifice. The amplitude of the random force is a function of time and all spatial coordianate directions. In order to determine a suitable amplitude for the perturbation, three different amplitudes are tested. Dimensionless forces $\underline{F}/(\rho d^2 (u_j - u_{co})^2)$

$$F_x = A(1.0 - 2.0X) \tag{15}$$

$$F_y = A(1.0 - 2.0X) \tag{16}$$

$$F_z = A(1.0 - 2.0X) \tag{17}$$

Where F_x, F_y and F_z are the forced in x_1, x_2 and x_3 directions, A is the amplitude and X is a random number and a function in time, space and direction and changes its values between 0 and 1. with amplitudes of $F = 10, 20$ and 50 are used.
For this preliminary test the simulations are started from a DNS in a relatively short (in x_3-direction) computational domain with a longitudinal size of $x_3/d = 20$ and a radial size of $x_3/d = 6$ discretized with 900 three dimensional spectral elements. The dependence of the forcing amplitude F is shown in figures 9, 10 and 11. As can be seen in figure 9 the mixing of the species increases with increasing amplitude. The same is true for the thickness of the shear layer, which is presented in figure 10 and for the intensity of the vorticity, see figure 11.

The self-similarity of the mean velocity of the jet is according to Lubbers et al. [13] reachead after around $x_3/d = 30$. The conclusion is, that the mean velocity profile does not yet reach the scale similarity at a longitudinal size of $x_3/d = 20$, however, we expected that the velocity profile would converge to the self similar profile in a longer domain. In figure 12 normalized velocity profiles are presented and it is obvious that the self-similarity is not yet reached.

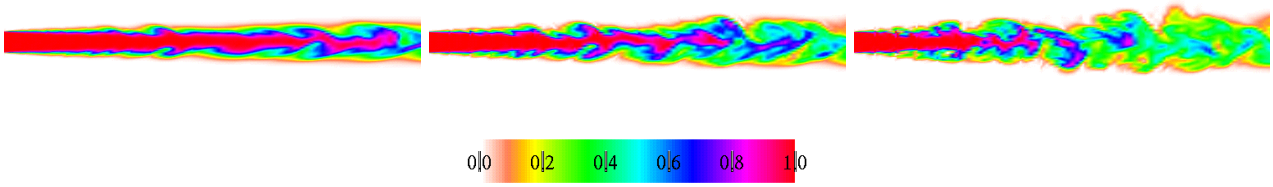

Figure 9: Fuel concentrations for $F = 10$ (left), $F = 25$ (middle) and $F = 50$ (right)

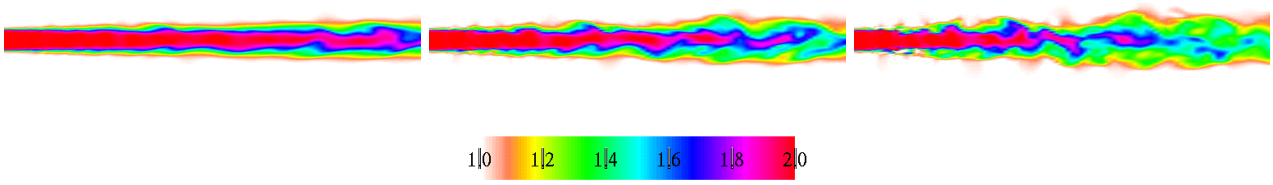

Figure 10: Streamwise velocity for $F = 10$ (left), $F = 25$ (middle) and $F = 50$ (right)

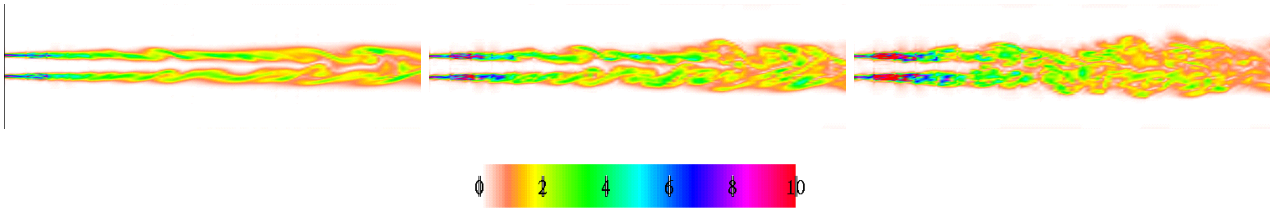

Figure 11: Vorticity for $F = 10$ (left), $F = 25$ (middle) and $F = 50$ (right)

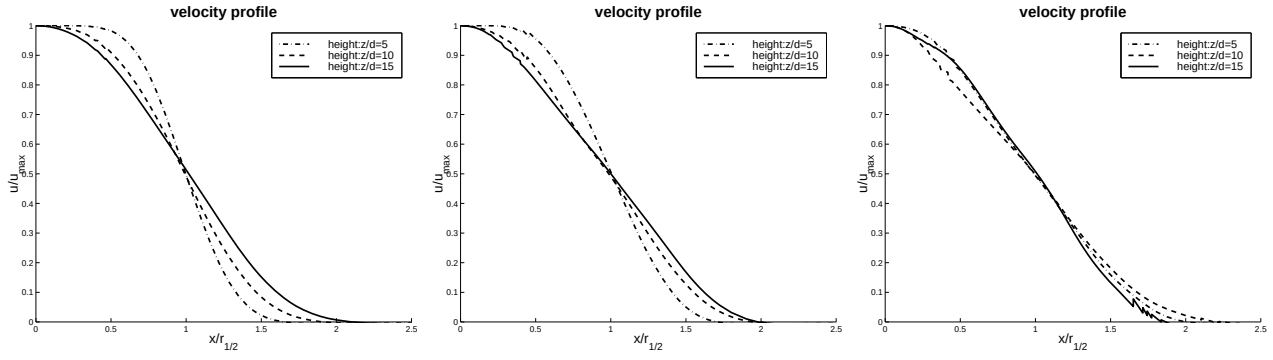

Figure 12: Nondimensional velocity profiles at different x_3-locations for $F = 10$ (left), $F = 25$ (middle) and $F = 50$ (right). u_{max} is the maximum centerline x_3-velocity and $r_{1/2}$ ist the radial distance of the mean velocity region.

4.4 Conclusions and Outlook

The setup for a mixing jet is done for the case of a DNS and first preliminary results show realistic results. A forcing is needed to get a turbulent jet. One possibility of the forcing is investigated, however, it seems not to be the best possibility. As a consequence following improvements are proposed :

- The computational domain length should be increased to $z/d = 40$
- A more realistic forcing-method should be used to perturbate the flow field

5 Bibliography

References

[1] Becker, H.A., Hottel, H.C., Williams, G.C., 1967. The nozzle fluid concentration field of the round turbulent jet. J. Fluid Mech. 30, 285-301.

[2] Borsma, B.J., Brethouwer, G., Nieuwstadt, F.T.M., 1998. A numerical investigation on the effect of the inflow conditions on the self-similar region of a round jet. Phys. Fluid Vol.10, No 4, 899-909.

[3] Bronstein, Semendjajew, Musiol, Mühlig. Taschenbuch der Mathematik. Verlag Harry Deutsch Thun und Frankfurt am Main. 3. Auflage 1997

[4] Capp, S.P. 1983. Experimental investigation of turbulent axisymmetric jet. PhD dissertation, University at Buffalo, SUNY.

[5] Corrosin, S., Uberoi, M.S., 1950. Further esperiments on the flow and heat transfer in a heated turbulent air jet. NACA report 998.

[6] Danaila, I., Dusek, J., Anselmet, F., 1997. Coherent structures in a round, spatially evolving, unforced, homogeneous jet at low Reynolds numbers. Phys. Fluids 9, 3323-3342.

[7] Dowling, D.R., Dimotakis, P.E., 1990. Similarity of the concentration field of gas-phase turbulent jet. J. Fluid Mech. 218, 109-141.

[8] Fischer, P.F., Mullen, J.S., 1999. Filter-based Stabilization of Spectral Element Methods. ??.

[9] George, W.K., Capp, S.P., Seif, A.A., Baker, C.B, Taulbee, D.B., 1988. A study of the turbulent axisymmetric jet. J. Engng. Sci. King Saud Univ. 14, 85-93.

[10] Hinze, J.O., 1975. Turbulence. McGraw-Hill, New York.

[11] Hussein, H.J., Capp, S.P., George, W.K., 1994. Velocity measurements in a high-Reynolds-number, momentum-conserving, axisymmetric, turbulent jet. J. Fluid Mech. 258, 31-75.

[12] Küng, M., 2003. Fluid Mechanic Notes. Internal Report, ETH Zürich Aerochemistry and Combustion System lab.

[13] Lubbers, C.L., Brethouwer, G., Boersma, B.J., 2001. Simulation of the mixing of a passive scalar in a round turbulent jet. Fluid Dyn. Res. 28, 189-208.

[14] Moser, R.D., Kim, J., Mansour, N.N., 1999. Direct numerical simultion of turbulent channel flow up to $Re_\tau = 590$. Phys. Fluids, 11(4), 943-945.

[15] Panchapakesan, N., Lumley, J.L., 1993. Turbulence measurements in axisymmetric jets of air and helium. Part 1. Air Jet. J. Fluid Mech. 246, 197-223

[16] Pope, S.B., 2000. Turbulent Flows. Cambridge University Press.

[17] Rodi, W. 1975. A new method of analyzing hot-wire signals in highly turbulent flow and its evaluation in a round jet. DISA Information. 17, Feb. 1975.

[18] Scheffer, R.E., Kerstein, A.R., Namazian, M., Kelly, J., 1994. Role of large-scale structure in a nonreacting turbulent CH_4 jet. Phys. Fluid 6, 652-661.

[19] Seif, A.A. 1981. Higher order closure model for turbulent jets. PhD Dissertation, University at Buffalo, SUNY.

[20] Stolz,S., Adams, N. A., Kleiser, L., 2001. The approximate deconvolution model for large-eddy simulations of compressible flows and its application to shock-turbulent-boundary-layer interaction. Phys. of Fluids, Vol.13 No. 10

[21] Vremani, B., 1995. Direct an Large-Eddy simulation of the compressible turbulent mixing layer. Dissertation ISBN 90-9008884-9. University of Twente

[22] Wygnansky, I., Fiedler, H. 1969. Some measurements in the self-preserving jet. J. Fluid Mech. 38, 577-612.

2. Non-premixed turbulent combustion modeling using large eddy simulation and unsteady flamelet models

Sevket Baykal, Jürg Gass

Laboratory of Thermodynamics in Emerging Technologies LTNT

LTNT

8092 Zürich, Switzerland

http://www.ltnt.ethz.ch

sevket.baykal@ltnt.iet.mavt.ethz.ch

8th December 2003

There are two classifications of reactions: premixed and nonpremixed, in order to conceptually simplify the problem of turbulent combustion, especially in the development and utilization of models. In premixed reactions, e.g., in an internal combustion engine, the premixed fuel and oxidant are ignited locally, for example by a spark. Turbulent nonpremixed flames are encountered in a large number of industrial systems for two main reasons. First, compared to premixed flames, burners are simpler to design and to build because a perfect reactant mixing, in given proportions, is not required. Nonpremixed flames are also safer to operate as they do not exhibit propagation speeds and cannot flashback.

The understanding and prediction of the behaviour of turbulent reacting flows is generally much more difficult than that for nonreacting flows. First of all the flow is usually compressible, so that, in addition to the conservation of mass and momentum and constitutive relationships, also the conservation of energy as well as gas laws must be considered. Furthermore, conservation equations for chemical species must be included, often for many chemical species and numerous chemical reactions. The reactions can result in large heat release, resulting, for example, in large temperature and density variations. There are varieties of combustion models that are being used by different groups in the combustion community. Using flamelet models has done the most of the calculations using complex chemistry in turbulent combustion.

1 Flamelet Modeling

The conservation equations for fuel, oxidizer and temperature can be written:

$$\frac{\partial}{\partial t}(\rho Y_F) + \frac{\partial}{\partial x_i}(\rho u_i Y_F) = \frac{\partial}{\partial x_i}\left(\rho D \frac{\partial Y_F}{\partial x_i}\right) + \dot{\omega}_F \tag{1}$$

$$\frac{\partial}{\partial t}(\rho Y_O) + \frac{\partial}{\partial x_i}(\rho u_i Y_O) = \frac{\partial}{\partial x_i}\left(\rho D \frac{\partial Y_O}{\partial x_i}\right) + s\dot{\omega}_F \tag{2}$$

$$\frac{\partial}{\partial t}(\rho T) + \frac{\partial}{\partial x_i}(\rho u_i T) = \frac{\partial}{\partial x_i}\left(\frac{\lambda}{C_p}\frac{\partial T}{\partial x_i}\right) - \frac{\Theta}{C_p}\dot{\omega}_F \tag{3}$$

Combining the equations from (1) to (3) one can find the following balance equation for the passive scalar, without source term:

$$\frac{\partial}{\partial t}(\rho Z)+\frac{\partial}{\partial x_i}(\rho u_i Z)=\frac{\partial}{\partial x_i}\left(\rho D\frac{\partial Z}{\partial x_i}\right) \tag{4}$$

Where Z is a passive (conserved) scalar and it is called mixture fraction. Mixture fraction is changed because of diffusion and convection but not reaction. Reaction still plays an indirect role in mixture fraction controlling temperature and, therefore, density and velocity fields. Basically mixture fraction measures the local fuel oxidizer ratio and it leads to:

$$Z=\frac{sY_F-Y_O+Y_O^o}{sY_F^o+Y_O^o} \tag{5}$$

Y_F^o And Y_O^o are fuel and oxidizer mass fractions in pure fuel and oxidizer streams respectively. Therefore, Z is equal to 1 in the fuel stream and zero in the oxidizer stream.

Experiments and DNS results in jet flames show that there are some situations in the burners that there is no more fast chemistry situation. Because of that using of the finite chemistry model is a must in most of the burners. Flamelet models were introduced for this requirement. These models are derived assuming that local balance between diffusion and reaction. Two control parameters of planar and steady laminar strained flames are used, the mixture fraction and its scalar dissipation rate. In turbulent flow, these two quantities fluctuate in space and time, but when the joint pdf $\tilde{P}(Z^*,\chi^*;x,t)$ is known, the mean properties of the flame may be calculated as:

$$\tilde{Y}_i=\int_{Z^*}\int_{\chi^*}Y_F(Z^*,\chi^*)\tilde{P}(Z^*,\chi^*;x,t)d\chi^*dZ^* \tag{6}$$

Yi is the local flame structure in mixture fraction space and $\tilde{P}(Z^*,\chi^*;x,t)$ captures the statistics of fuel-air mixing. The inputs of steady laminar flamelet model are similar to infinitely fast chemistry presumed pdf model .In addition to $\tilde{Z}$ and $\tilde{Z}''^2$, the scalar dissipation rate is used to include the finite rate chemistry effects. An increase in χ is followed by finite chemistry effects, or even quenching when χ becomes too large. For a given chemical time, if Damkohler number is large enough the last equation may cover infinitely fast chemistry solution. In (6) Yi(Z, χ) may be tabulated from solutions of counter-flow diffusion flames.

The assumption that is used here can be verified multiple ways refer to Williams (1985) and Peters (1984). All the derivations used in literature imply that the flame structure locally one-dimensional and depends only on time and on the coordinate normal to the flame front (or on iso surface of Z). In a multi dimensional flow, this assumption requires that the flame be thin compared to the other flow and wrinkling scales. Each element of the flame front can then be viewed as a small laminar flame also called flamelet. The flamelet definition is the basis of many models for turbulent combustion. Peters (2000) defines the flamelets are thin reactive diffusive layers embedded within an otherwise nonreacting turbulent flow field. If one assumes the thin quasi one-dimensional structures convected and stretched by the fluid motions, and neglecting higher order terms, the equations for the species and temperature become:

$$\frac{\partial Y_i}{\partial t}=\dot{\omega}_i+\left(\frac{\chi}{Le_i}\right)\left(\frac{\partial^2 Y_i}{\partial Z^2}\right) \tag{7}$$

$$\frac{\partial T}{\partial t}=-\sum_{n=1}^{N}\frac{h_n\dot{\omega}_n}{C_p}+\chi\left(\frac{\partial^2 T}{\partial Z^2}\right) \tag{8}$$

Where the scalar dissipation rate χ is introduced:

$$\chi = 2D\left(\frac{\partial Z}{\partial x_i}\frac{\partial Z}{\partial x_i}\right) \tag{9}$$

Equation (7) and (8) are called flamelet equations. The extended form of these equations can be found in the literature, Peters (1984), and Pitsch & Peters (1998). In these equations the only term depending on spatial variables is the scalar dissipation rate. Scalar dissipation rate has the dimension of an inverse time. It measures the Z-gradients and the molecular fluxes of species towards the flame. It controls the mixing because it controls the gradients of Z. It is directly influenced by strain, when strain rate increases, χ increases.

Once χ is specified, the flamelet equations can be solved in Z space to provide the flame structure, i.e. the temperatures and species as functions of mixture fraction Z and time t.

For steady flamelet case and for a given value of χ corresponding to local micro mixing conditions, one has to solve (10).

$$\dot{\omega} = -\frac{\chi}{Le_i}\frac{\partial^2 Y_i}{\partial Z^2} \tag{10}$$

The solution of this equation for given concentrations and temperatures boundary conditions, and various χ provides a Flamelet Library Yi (Z, χ).

The steady laminar flamelet approach assumes that the characteristic time required balancing diffusion and reaction is smaller than any other flow time scale of the problem. In this method: The turbulent micro mixing of chemical species does not need any particular treatment, since diffusion is directly induced and coupled with chemistry in (10).

Eqn. (10) has been obtained neglecting diffusion in the direction tangential to the iso surface Z_{st} surface, arguing that when the mixing element is sufficiently thin and features weak curvature, the gradients measured along stoichiometric surface are much smaller than those in the perpendicular direction.

In steady laminar flamelet models, the fuel-air turbulent mixing is captured via joint pdf $\tilde{P}(Z^*, \chi^*; x, t)$. Most of the flamelet models explicitly suppose that the mixture fraction and its dissipation rate are two uncorrelated quantities.

$$\tilde{P}(Z^*, \chi^*; x, t) \approx \tilde{P}(Z^*; x, t)\tilde{P}(\chi^*; x, t) \tag{11}$$

$\tilde{P}(Z^*; x, t)$ is presumed to follow a β function, whose shape is determined by the mean and sub-grid scale variance of the mixture fraction. The filtered mixture fraction is determined by the solution of a transport equation; its sub-grid scale variance is typically given by a sub-grid scale model by Pitsch (2000), Pierce and Moin (1998). Sub-grid scale mixture fraction variance is modelled as;

$$\bar{\rho}\widetilde{Z''^2} = C_Z \Delta^2 \bar{\rho}\left|\nabla \tilde{Z}\right|^2 \tag{12}$$

where the coefficient C_Z is determined using the dynamic procedure.

The validity of the β function representation of the pdf of the mixture fraction has been investigated by several authors using DNS data of nonpremixed reacting flows for constant and variable density Cook (1997) and Wall (2000). The main conclusion should be noticed here that β function pdf provides an excellent estimate for the sub-grid scale mixture fraction distribution and that this estimate is much better for LES than for RANS models Pitsch (2000).

1.1 Unsteady Flamelet Approach

When a high value of the scalar dissipation rate is imposed to the flame for a sufficiently short period of time, extinction may not be completed, with limiting frequency at which the flame almost behaves like a steady state flame. Unsteady flamelets is used to simulate extinction and reignition in a turbulent jet flame, history effects may be included using a Lagrangian time measured along the stoichiometric line.

In the configuration of the jet flames; if we focus on the inlet, pure air and pure fuel react to form products. Moving downstream, turbulent diffusion mixes these products with air, on the airside, and with fuel, on the fuel side. Further downstream, the reactants feeding the reaction zone are not likely to be either pure fuel or pure air. This situation is strongly enhanced in flows where recirculation zones are found to stabilize combustion Ferreira (1996). This reality may be modelled by using a progress variable c as a parameter in the transient flamelet libraries.

When partially premixed flamelets are expected in the combustion system, for instance at the base of a lifted turbulent jet-flame, it may be interesting in the modelling to use premixed flamelets instead of diffusion flamelets. Using a progress variable in the transient flamelet libraries may also solve partially premixed flamelets. The mass fractions and temperatures are parameterized in terms of the mixture fraction, characteristic time, scalar dissipation and progress variable terms.

2 The Model

In the present study a sub-grid scale model is introduced for the scalar dissipation rate in non-premixed turbulent reacting flows. The scalar dissipation and its dependency on laminar and turbulent fields are described by using scalar and vectorel quantities estimated locally from the Favre-filtered field. The unsteady flamelet equations for species and temperature are solved using the FLATRA code Ferreira (1996).

The transient laminar flamelet model (TLFM) is based on four variables. In addition to the mixture fraction Z and the scalar dissipation rate χ, which are used for the steady laminar flamelet model, a flamelet development time τ and a reaction progress variable c are introduced. The transported value $\tilde{C}$ governs the further development of the laminar flamelet and the value handle the mixing of an extincted state and the transient re-ignition separately. In the following paragraphs the definitions of these parameters can be found.

The instantaneous scalar dissipation rate generally defined as in Eqn. (9). In the proposed method this diffusivity has been altered by molecular and turbulent diffusivities of species

$$\chi = C_1\left(D_m + D_t\right)\left(\nabla Z\right)^2 \tag{13}$$

where Dm and Dt represent molecular and turbulent diffusivities respectively. In this study, the molecular diffusion dependency of scalar dissipation is predicted based on well-known Chapman-Enskog kinetic theory by using Fuller et.al. empirical relation (1997). In the formula molecular diffusion coefficient express in terms of temperature, pressure, molecular weight of species and diffusion volumes of molecules. This theory is accurate to an average of about eight percentages.

$$D_m = 10^{-3}\frac{T^{1.75}\left(1/\tilde{M}_1 + 1/\tilde{M}_2\right)^{1/2}}{p\left[\left(\sum_i V_{i1}\right)^{1/3} + \left(\sum_i V_{i2}\right)^{1/3}\right]^2} \tag{14}$$

In order to define the turbulent part of scalar dissipation equation sub-grid diffusivity equation is proposed. The Kolmogorov length and time scales are smallest scales occurring in turbulent motion. These scales decrease with increasing dissipation rates. The small-scale motion is quite viscous and the viscous dissipation adjusts itself to the energy supply by adjusting length scales. Therefore the sub-grid diffusivity can be determined from turbulent viscosity and a constant turbulent Schmidt number.

$$D_t = \frac{\upsilon_t}{S_c} \tag{15}$$

turbulent viscosity is defined by subgrid model

$$\nu_t = (C_s\Delta)^2(2\bar{S}_{ij}\bar{S}_{ij})^{1/2} \quad \propto \Delta^2 \tag{16}$$

The mean value of the reaction progress variable is also obtained with an additional transport equation as:

$$\frac{\partial\bar{\rho}\tilde{c}}{\partial t} + \frac{\partial\bar{\rho}\tilde{u}_j\tilde{c}}{\partial x_j} = \frac{\partial}{\partial x_j}\left\{\left(\bar{\rho}D + \frac{\mu_t}{Sc_t}\right)\frac{\partial\tilde{c}}{\partial x_j}\right\} + \bar{S}_c \tag{17}$$

$$\bar{S}_c = \frac{1}{\tau}\cdot(c_{fl} - \tilde{c}) \qquad \text{if} \quad c_{fl} - \tilde{c} > 0$$
$$\bar{S}_c = 0 \qquad \text{if} \quad c_{fl} - \tilde{c} < 0 \tag{18}$$

$\tilde{c}$ and c_{fl} are defined by :

$$c_{fl} = \frac{Y_{F,u}(Z) - Y_F(Z,\chi.\tilde{c},\tau)}{Y_{F,u}(Z) - Y_{F,b}(Z)} \tag{19}$$

$$\tilde{c}(Z) = \frac{Y_{F,u}(\tilde{Z}) - Y_F(\tilde{Z})}{Y_{F,u}(\tilde{Z}) - Y_{F,b}(\tilde{Z})} \tag{20}$$

where F ,u, b denotes fuel, burned state and unburned state respectively.

Flamelet development time is introduced as:

$$\tau = C_\tau \frac{\sqrt[3]{CV_{grid}}}{\bar{V}} \qquad \text{with} \qquad C_\tau \approx 1 \tag{21}$$

where CV_{grid} is the grid control volume.

The mean mass fractions of the chemical species $\tilde{Y}_n$ and the temperature $\tilde{T}$ are defined as:

$$\tilde{Y}_n = \int_0^1\int_0^1\int_0^\infty\int_0^\infty Y_n(Z,c,\chi,\tau).P(Z,c,\chi,\tau)dZ\,dc d\chi\,d\tau \tag{22}$$

$$\tilde{T} = \int_0^1\int_0^1\int_0^\infty\int_0^\infty T(Z,c,\chi,\tau).P(Z,c,\chi,\tau)dZ\,dc\,d\chi\,d\tau \tag{23}$$

3 The Case

The burner geometry used in this study is general burner geometry for the piloted flames at Sydney University and Sandia (Fig1). The jet fluid is mixture of three parts air and one part CH4 by volume. The pilot is a lean (λ=0.77) mixture of C2 H2, H2, air, CO2 and, N2 with the same nominal enthalpy and equilibrium composition as methane/air at equivalence ratio. The mixing rates are high enough that these flames burn as

diffusion flames, with a single reaction zone near the stoichiometric mixture fraction. The Flame D (Re=22400) is used as a test case in the model study, has a small degree of local extinction (11).

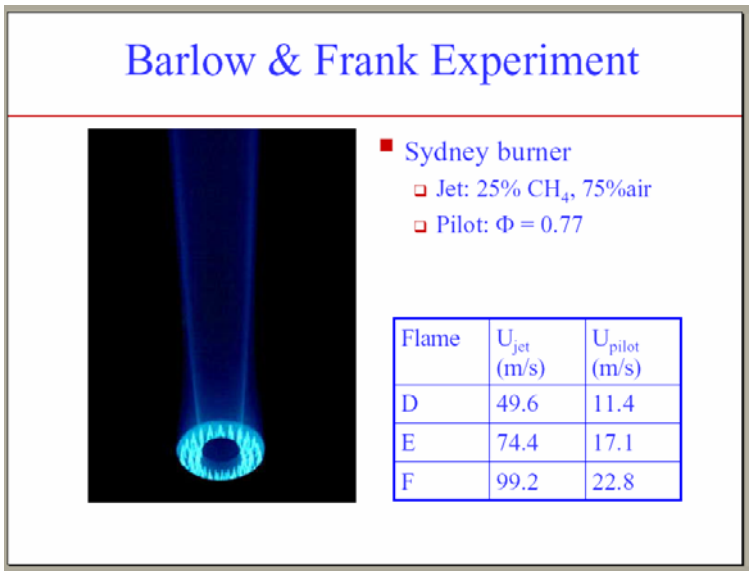

Fig.1 Sandia Flame D

In this study the LTNT's flamelet code has been implemented to the new flow solver CFX5.6. The run has been submitted. The result will be ready to check in coming weeks. The optimization studies in terms of cost efficiency have been started.

4 References

1.Williams, F. A. (1985). Combustion theory, Benjamin/Cummins, Menlo Park, CA.

2.Peters, N. (1984). Laminar diffusion flamelet models in non-premixed turbulent combustion, Prog. Energy Combust. Sci. 10, 319-339.

3.Peters, N. Wenzel, H., and Williams, F. A. (2000). Modification of the turbulent burning velocity by gas expansion effects, Proceedings of the Combustion Institute, Vol. 28, 235-243.

4.Pitsch, H. and Peters, N. (1998). A consistent flamlet formulation for non-premixed combustion considering differential diffusion effects, Combst. Flame 114, 26-40.

5. Pitsch, H and Steiner, H. (2000). Large-eddy simulation of a turbulent piloted methane air diffusion flame (Sandia Flame D), Phys. Fluids, vol. 12, no. 10, pp. 2541-2554.

6. Pierce, C. D. and Moin, P. (1998). A dynamic model for subgrid-scale variance and dissipation rate of a conserved scalar, Phys. Fluids, vol. 10, pp.3041-3044.

7.Cook, A. W., Riley, J. J., and Kosaly, G. (1997). A laminar flamelet approach to subgrid-scale chemistry in turbulent flows, Combust. Flame 109, 332-341.

8. Wall, C., B.J. Boersma & P. Moin(2000). An evaluation of the assumed beta probability density function subgrid-scale model for large eddy simulation of nonpremixed, turbulent combustion with heat release, Physics of fluids, 12, 10, p.p. 2522-2529.

9.Ferreria, J.C., (1996). Flamelet modelling of stabilization in turbulent non-premixed combustion, Dissertation.

10. Cussler E. L. (1997). Diffusion Mass Transfer in Fluid Systems, Cambridge University Press.

11. Barlow, R. S., and Frank J.H., (1998). Proc. Comb. Inst. 27:1087

3.) Large Eddy Simulation of Non-premixed Combustion using a High-order, Truly Multidimensional Compressible Fluid Solver and PDF Combustion

Part 1. A Truly Multidimensional Transport Method

Part 2. The LES Equations and the Sub-grid Models

M. Sc. Julian T. Becerra Sagredo and Prof. Rolf Jeltsch

Seminar of Applied Mathematics SAM

SAM

8092 Zürich, Switzerland

http://www.sam.math.ethz.ch

julian@math.ethz.ch

1 Introduction

Large Eddy Simulation is a numerical tool where the large vortex structures in a fluid are solved explicitly over a coarse mesh. It is important that the numerical method used to simulate the dynamics of these structures produces very low numerical diffusion. Large numerical diffusion could induce large errors into the sub-grid structures.

In Finite Volume methods one source of large numerical diffusion is the straightforward dimensional splitting of the equations in each coordinate direction. The cross derivatives are simply not taken into account in the numerical approximations and therefore the numerical errors are dependent on the flow direction. Even if one-dimensional high order schemes are used in each direction, the overall accuracy is still low due to the lack of fluxes through the corners. The finite character of the fluid elements and the discrete time steps force the schemes to include the multidimensionality in a coupled manner. The original idea of simple one-dimensional splitting of the equations is valid only in the analytic limit when the volume of the elements is zero.

It has been investigated at the Seminar of Applied Mathematics of the ETH-Zurich, that the spatial splitting of fluxes used in multidimensional finite volume codes is not truly multidimensional and produces large errors (numerical diffusion) when the main flow direction is not inline with the coordinate directions. A solution to this problem is the Method of Transport (MoT) [2], where truly multidimensional fluxes are computed. Unfortunately, this method contains complicated expressions if high-order accuracy is to be achieved.

Following the same philosophy of the MoT, we propose the development of a compressible Lagrangian-transport method (LTM). In this method the equations are integrated along fluid element trajectories represented by Lagrangian Finite Volumes. In one discrete time step these volumes deform and an explicit algebraic mapping is used to interpolate the transported quantities back to a fixed Cartesian mesh.

During this research we have discovered the complete Orthonormal Spline Basis that we have named Z-splines. They are the unique piecewise polynomial solution to the general interpolation problem of minimum compact support, and successive maximum smoothness and accuracy.

All the fluid properties are represented by the Z-spline basis. The Z-splines provide a stable and highly accurate extension of the discrete fluid properties to the continuous space and therefore any source term given in

integral or differential form is computable in perfect consistency with the numerical representation. In this context, the source terms are computed with multidimensional finite difference approximations and interpolated to the discrete positions along the trajectories. The same interpolation technique is used to reinitialise the fields at the end of a Runge-Kutta integration step in order to avoid further problems due to large Lagrangian-grid distortion. The mapping and the interpolation are achieved with the Z-spline functions. The Lagrangian Transport Method (LTM) is truly multidimensional, local, explicit, high order in time and space, and produces negligible numerical diffusion. Domain decomposition for parallel processing with the MPI standard and immersed boundaries to represent complex geometries are straightforward.

The compressible Navier-Stokes equations are discretized using the LTM. Large Eddy Simulation is been developed using a sub-grid kinetic energy turbulence model. The combustion model is based on a Lagrangian Probability Density Function formulation that reduces the number of equations needed to simulate the chemical reactions.

Results are available for the simulation of the compressible Navier-Stokes equations and the use of the combustion model using a commercial incompressible fluid solver.

2 Truly Multidimensional High-order Langrangian Transport Method

The Lagrangian Transport Method is based on the solution of the non-homogeneous transport equation

$$\frac{d}{dt}a(x,t) = \frac{\partial}{\partial t}a + u \cdot \nabla a = f(x,t)$$

where the velocity field $u=u(x,t)$ is used to integrate the Lagrangian trajectory of every point in the domain, given by the characteristic equations

$$\frac{d}{dt}x(x_0,t) = u(x,t)$$

The scalar function $a=a(x,t)$ is constant along the trajectory if $f(x,t)=0$.

In the numerical method, the fields $a=a(x,t)$ and $u=u(x,t)$ are represented on a three-dimensional Cartesian mesh. The integration of the trajectory of every point on the mesh is done with an explicit Runge-Kutta method. After every time step the "moved" field $a=a(x,t)$ has the be interpolated back to the original Cartesian mesh in order to avoid too much deformation of the fluid elements and therefore the divergence of the method. The elements are then re-initialized on the Cartesian mesh after every time step.

A1 Interpolation from the deformed mesh

The interpolation from the "deformed" Lagrangian Finite Volumes is achieved through the inversion of a non-linear mapping. The Lagrangian Finite Volumes are defined by the coordinates of the *8* corner points (for a linear Z-spline Finite Volume), *64* neighboring points (for a cubic Z-spline Finite Volume), or more points for higher order Z-splines. The coordinates of the corners in the mapped space $\xi=(\xi,\eta,\zeta)$ are defined as integer numbers on a Cartesian mesh, such that, in order to represent a point $x=(x,y,z)$ given $\xi=(\xi,\eta,\zeta)$, it is necessary to use the cardinal Z-spline interpolation formula of order $2m-1$

$$x(\xi,\eta,\zeta) = \sum_i x(\xi_i,\eta_i,\zeta_i) Z_m(\xi-\xi_i) Z_m(\eta-\eta_i) Z_m(\zeta-\zeta_i)$$

where $x(\xi_i,\eta_i,\zeta_i)$ are the coordinates of the corners of the Lagrangian Finite Volumes.

Any point inside each Lagrangian Finite Volume can be represented in the coordinates $\Delta\xi=(\Delta\xi,\Delta\eta,\Delta\zeta)$ through the inversion of a non-linear mapping given by the Taylor series expansion around the local Lagrangian coordinates $\xi=(0,0,0)$

$$\Delta x = x_\xi\Delta\xi + x_\eta\Delta\eta + x_\zeta\Delta\zeta + x_{\xi\eta}\Delta\xi\Delta\eta + x_{\xi\zeta}\Delta\xi\Delta\zeta + x_{\eta\zeta}\Delta\eta\Delta\zeta + x_{\xi\eta\zeta}\Delta\xi\Delta\eta\Delta\zeta + \ldots$$
$$\Delta y = y_\xi\Delta\xi + y_\eta\Delta\eta + y_\zeta\Delta\zeta + y_{\xi\eta}\Delta\xi\Delta\eta + y_{\xi\zeta}\Delta\xi\Delta\zeta + y_{\eta\zeta}\Delta\eta\Delta\zeta + y_{\xi\eta\zeta}\Delta\xi\Delta\eta\Delta\zeta + \ldots$$
$$\Delta z = z_\xi\Delta\xi + z_\eta\Delta\eta + z_\zeta\Delta\zeta + z_{\xi\eta}\Delta\xi\Delta\eta + z_{\xi\zeta}\Delta\xi\Delta\zeta + z_{\eta\zeta}\Delta\eta\Delta\zeta + z_{\xi\eta\zeta}\Delta\xi\Delta\eta\Delta\zeta + \ldots$$

The displacements $(\Delta x, \Delta y, \Delta z)$ are known. The derivatives at $\xi=(0,0,0)$, including all cross derivatives, are computed through the products of the derivatives of the corresponding multidimensional Z-splines.

The non-linear mapping given by the Taylor series expansion is inverted using Newton's method in three dimensions. The values of $\Delta\xi=(\Delta\xi,\Delta\eta,\Delta\zeta)$ are computed up to machine precision in a few iterations (typically four). The initial guess is given by the direct inversion of the linear problem without the cross-derivatives.

The *routine* to compute $\Delta\xi=(\Delta\xi,\Delta\eta,\Delta\zeta)$ must check if the computed coordinates lie on the interval $[0,1)$ and, if out of bound, the it computes them again inside the correct Lagrangian Finite Volume.

2.1 The LES Equations and the Sub-grid Models.

The LES equations for a compressible fluid with a sub-grid kinetic energy dynamic turbulence model can be found in [7].

The LTM is used to solve these equations. In order to be able to use the LTM, the equations are written using the total time derivative and treating the other terms as sources.

The source terms in the right hand side are discretized using the finite differences corresponding to the Z-spline used for the interpolations.

CFL numbers should be monitored to achieve stability.

The LES of the compressible Navier-Stokes equations requires some special numerical procedures that have been investigated and improved during our research. The Z-spline basis functions have been used to develop a high-order explicit diffusion method, a high-order non-diffusive, non-dispersive filtering procedure and a numerically exact conservative transport.

The high-order explicit diffusion method is based on the exact solution of the heat equation with a singular source [6]. The Z-spline heat kernel is computed numerically using the convolution of a single Z-spline with the heat kernel. The resulting scheme is highly accurate for small time steps or small diffusion coefficients (typical for the coarse mesh LES) and unconditionally stable.

The Z-splines are used to develop a filtering procedure that is non-diffusive and non-dispersive. The fourier transforms of the Z-splines are successive approximations to the perfect reconstruction filter. The filtering procedure is based on interpolation using coarser set of points and averaging.

Periodic boundary conditions and non-reflective open-field boundary conditions have been investigated. The non-reflective condition is obtained using a reflection zone combined with a strong filtering procedure near such a boundary.

3 The PDF Combustion Model

The combustion model is being tested and developed by the group of the Laboratory of Thermodynamics in Emerging Technologies LTNT-IET.

4 Results

4.1 The Orthonormal Piecewise Polynomial Basis: Z-splines

The complete family of orthonormal piecewise polynomials has been discovered as a sub-product of this research. The basis consists of Hermite-Birkhoff curves $Z_m=Z_m(x)$ of degree and order $2m-1$ that represent explicit finite differences computed by Taylor series expansions. One-sided Z-splines and arbitrary-interval Z-splines have been also engineered such that the Z-splines are the explicit solution to the general interpolation problem.

A publication of the general theory of the Z-splines has been prepared for submission. In the paper a detailed analysis of their properties is achieved. The Z-splines are the unique piecewise polynomial solution to the general interpolation problem of minimum compact support and successive maximum accuracy and regularity (smoothness). It has been proven that the following properties are equivalent for the Z-splines:

They represent exactly polynomials of degree or equal than *2m-2*.

They conserve the first *2m-1* discrete moments of the interpolated data.

They have unity zero integral moment and *2m-2* vanishing higher integral moments.

They have *(2m-1)*-th order of accuracy.

Their Fourier transform is unity at wave number zero and has zeroes of order *2m-1* at the multiples of *2*□.

They are the best piecewise polynomial approximation to the perfect reconstruction filter *sinc(x).*

The properties of the Z-splines have also been observed numerically. The easiest test is the vanishing moments property. A graphic representation of the theory of the orthonormal piecewise polynomial basis is presented in Fig. 1.

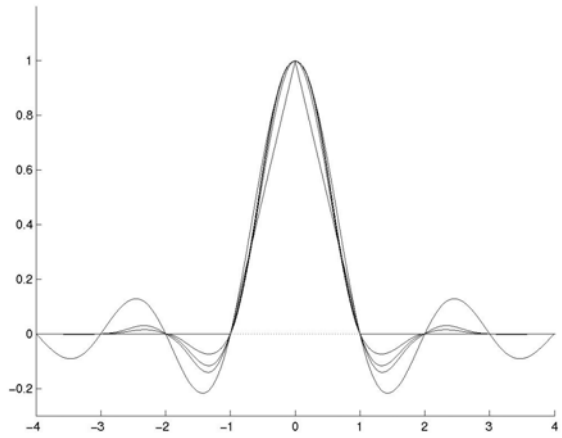

Figure 1. The first four z-splines and the sinc(x).

4.2 Convergence of the High-order Lagrangian Transport Method

The convergence of the high-order Lagrangian Transport Method has been observed numerically. The code has been named *LESReact* and it has been tested for the case of inviscid Green-Taylor vortices given by

$$u = -2\pi \cos(2\pi x)\sin(2\pi y)$$

$$v = 2\pi \sin(2\pi x)\cos(2\pi y)$$

$$w = 8\pi^2 \cos(2\pi x)\cos(2\pi y)$$

where u and v are the horizontal and vertical velocity components and w is the vorticity. The convergence of the method is observed computing the L_2-error of the analytic solution (invariant of time) compared with the

numerical solution after one time step for a fixed CFL = 0.5. The results are shown in Fig.2 for linear Finite Volumes (solid line) and cubic Finite Volumes (dashed line). Linear, cubic and fifth order interpolations are compared.

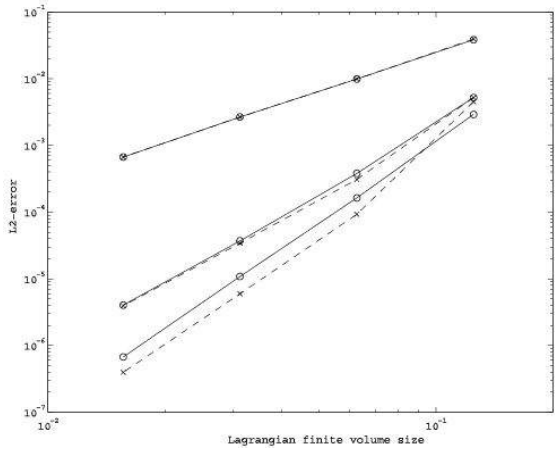

Figure 2. Convergence of the lagrangian transport method for linear (solid line) and cubic (dashed line) elements.

4.3 Filtering

The filtering procedure using Z-splines has been tested on a noisy signal made of steps. The LES method uses the filter to obtain a smooth function on the coarse grid to which the LTM integration can be applied. Fig. 3 shows the results for the fifth order Z-spline.

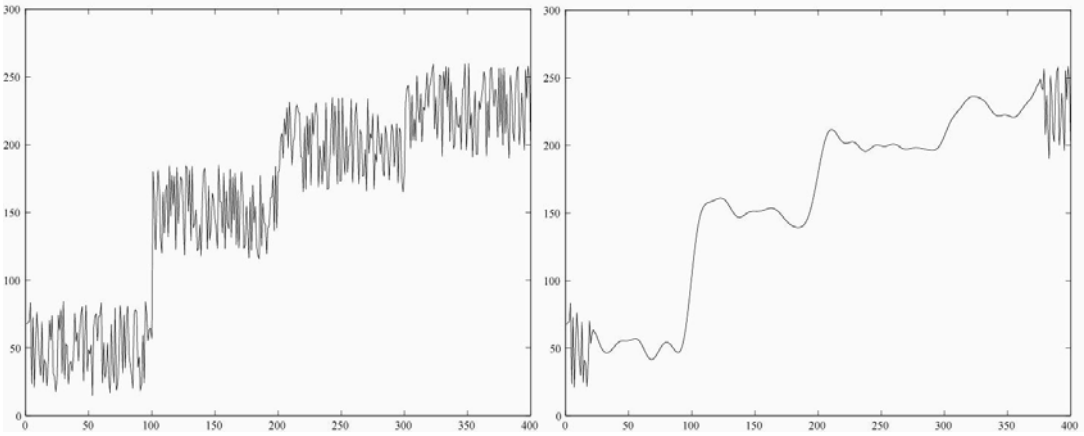

Figure 3. signal with noise (left) and fifth order z-spline filtering (right).

4.4 The compressible fluid solver

The compressible Navier-Stokes equations are solved using the LTM described in this report. The system of equations is solved fully coupled using high-order Runge-Kutta trajectory integrators. Simple three-dimensional acoustic waves have been used to test the code. An successful open-field boundary condition has been developed using a reflective zone combined with strong filtering near the boundary. The LES models based on dynamic eddy viscosity and a sub-grid kinetic energy transport equation as described in [7] are being implemented.

5 Summary 2003 and Future Plans

The discovery of the orthonormal piecewise polynomial basis has allowed to construct a high-order, truly multidimensional, Lagrangian transport method. The low numerical diffusion of this method is a strong basis for a Large Eddy Simulation code. The compressible fluid solver is based on the analytic representation of the physical variables given by the Z-splines. Differentiation and integration are done analytically, reducing to the application of convolution kernels. The compressible fluid solver has been tested for acoustic waves and non-reflective boundary conditions have been developed. The sub-grid models for LES are being implemented.

The near future plan consists in the final combination of this code with the PDF combustion routines of the group at the Laboratory of Thermodynamics and Emerging Technologies LTNT at ETH to obtain a highly accurate combustion solver.

6 References

[1] Becerra Sagredo, J. T., (2003) **"Z-splines: Moment Conserving Cardinal Spline Interpolation for Arbitrary Spaced Date"**, *submitted to Numerische Mathematik*

[2] Fey, M., (1993) **"Ein echt mehrdimensionales Verfahren zur Lösung der Eulergleichungen"**, *PhD. Thesis*, ETH Nr. 10034.

[3] Schoenberg, I. J., (1973) **"Cardinal Spline Interpolation".** Philadelphia, PA: SIAM, 1973.

[4] Whittaker, E. T., (1915) **"On the functions which are represented by the expansions of interpolation theory"**, in *Proc. R. Soc. Edinburgh*, vol. 35, pp. 181-194.

[5] Meijering, E., (2002) **"A Chronology of Interpolation: From Ancient Astronomy to Modern Signal and Image Processing"**, *Proceedings of the IEEE*, Vol. 90, No. 3, pp. 319-342.

[6] Kevorkian, J., (1990**) "Partial Differential Equations: analytical solution techniques",** Chapman and Hall, London UK, 1990.

[7] Kim, W.-W., Menon, S., and Mongia, H. C., (1999) "Large Eddy Simulations of a Gas Turbine Combustor Flow", *Combustion Science and Technology*, Vol. 143, pp. 25-62.